Molten Fuel-Coolant Interactions: Recent Analysis of Experiments

M. L. Corradini, N. A. Evans, and D. E. Mitchell
University of Wisconsin, Department of Nuclear Engineering
Madison, Wisconsin 53706

Received February 28, 1983
Accepted October 7, 1983

If a complete failure of normal and emergency coolant flows occurs in a light water reactor, fission product decay would eventually cause melting of the reactor fuel, leading to contact with water. An energetic fuel-coolant interaction (steam explosion) may result. Experiments were performed at Sandia National Laboratories in which ~5 to 20 kg of molten fuel simulant were delivered into water in which the water mass was 1.5 to 50 times greater than the fuel. These experiments in subcooled and saturated water showed that spontaneous explosions occurred over the range of water/fuel mass ratio and that in certain experiments multiple explosions occurred. The kinetic energy conversion ratio was <2%. A model is proposed to describe the fuel-coolant mixing process. The model is compared to these intermediate-scale experiments. Additional data analysis indicates that the steam explosion is affected by the mixing process.

INTRODUCTION

Given the absence of adequate cooling water to the core of a light water reactor (LWR), the fission product decay heat would eventually cause the reactor fuel and cladding to melt. This could lead to slumping of the molten core materials into the lower plenum of the reactor vessel, possibly followed by failure of the vessel wall and pouring of the molten materials into the reactor cavity. Recent analyses[1-5] have indicated that residual water is likely to be present both in the lower plenum and in the reactor cavity. Therefore, when the molten core materials enter either region, there is a strong probability of molten core contacting water. The physical process by which the molten core ("fuel") contacts and mixes with the water ("coolant") is important for three reasons:

1. It has the potential for rapid steam generation from a fuel-coolant interaction (FCI) either energetic (steam explosion) or nonenergetic (steam spike).
2. It is a source of combustible hydrogen from the oxidation of the metallic components of the molten core (e.g., iron, chromium, and zirconium).
3. It will affect the size of the fuel debris.

---

[1] L. D. BUXTON, "Molten Core-Water Contact Analysis," SAND77-1842, Sandia National Laboratories (1979).

[2] W. B. MURFIN, Ed., "Report of the Zion/Indian Point Study: Volume 1," SAND80-0617/1, NUREG/CR-1410, Sandia National Laboratories (1980).

[3] J. F. MEYER et al., " Preliminary Assessment of Core Melt Accidents at the Zion and Indian Point Nuclear Power Plants and Strategies for Mitigating Their Effects," NUREG-0850, Vol. 1, U.S. Nuclear Regulatory Commission (1981).

[4] G. KLOPP et al., *Zion Probabilistic Safety Study*, Commonwealth Edison Company (1981).

[5] R. E. HENRY et al., *Trans. Am. Nucl. Soc.*, **39**, 368 (1981).

This paper focuses on recent FCI experiments [designated Fully Instrumented Test Series (FITS)] conducted at Sandia National Laboratories[6,7] (SNL). These FCI experiments are characterized by

1. fuel mixing with the coolant in a drop model of contact
2. triggering of the explosion before or at base contact
3. propagation of the explosion through the fuel-coolant mixture producing high pressure coolant vapor
4. expansion of the explosion products producing mechanical work.

First, the experimental apparatus used by the SNL personnel is described. Then data from the fuel-coolant mixing phase are analyzed and criteria are proposed for limits for fuel-coolant mixing. Finally, the explosion data are presented and analyzed relative to the explosion conversion ratio, chamber pressurization, and the debris generated.

EXPERIMENTAL APPARATUS

The FITS experiments[6,7] were conducted both outside and in a containment chamber (Fig. 1). The earlier tests outside the chamber were performed to perfect instrumentation and melt delivery techniques (MD and MDC series) while mixing behavior was observed; the in-chamber experiments allowed more detailed measurements of the explosion conversion ratio, chamber pressurization, and the collection of the explosion debris.

The water interaction chambers used were designed such that water volumes were in the form of rectangular parallelepipeds, with square cross-sectional areas and open tops. These were fabricated from clear 6.3-mm-thick Plexiglas (methyl methacrylate) stock in sizes calculated to result in initial water-to-fuel mass ratios of 1.5:1 to 50:1.

The in-chamber experiments were instrumented with pressure transducers in the water chamber base and side walls to measure water phase pressure, in the chamber upper head to study debris slug characteristics, and in the FITS chamber side wall ports to measure the gas phase pressure. Melt delivery was initiated automatically through the use of probes in the crucible that sensed when the thermite reaction was complete. Melt entry time was measured by photodiodes 2.5 cm above the water surface; shape and velocity of the melt at water impact and during mixing were recorded by high-speed cameras. Debris recovered from the experiments was characterized by sieving, using sieve sizes ranging from 38 μm to 25 mm.

The fuel used in these experiments was prepared by a metallothermic (thermite) chemical reaction. The resulting fuel melt consisted of either iron alumina (55 wt% iron, 45 wt% alumina) or Corium (CORIUM-A+R; UO_2-ZrO_2-70 wt%, stainless steel-30 wt%) at a theoretical (maximum) temperature of 3100 K. This corresponds to an internal energy content of 3.3 MJ/kg for iron alumina and 1.8 MJ/kg for the Corium. Calorimetry tests indicated that the actual fuel internal energy was ~90% of this value.[6,7] This suggests a fuel melt entry temperature into the water pool of ~2800 K; this value is in agreement with optical pyrometer measurements made in a few tests. The iron alumina was used more extensively in these tests because it is an inexpensive high-temperature simulant for the actual fuel melt (Corium).

Water from the local water supply was used as the coolant. No special treatment, such as degassing or deionizing, was done. Water temperature was not controlled for the majority of the experiments and was between 309 and 319 K. Three experiments were done with saturated water at 368 K.

FUEL-COOLANT MIXING

Past research into fuel-coolant mixing (sometimes called "premixing") has been directed at predicting the physical limits for which mixing could or could not occur. Fauske[8] and Henry and Fauske[9] originally proposed that the fuel-coolant interface temperature on liquid-liquid contact must exceed the spontaneous nucleation temperature (approximately equal to the homogeneous nucleation temperature) to allow premixing and an energetic FCI; the homogeneous nucleation temperature for water is 583 K. The physical picture was that stable film boiling is established above this limit for a liquid-liquid system, and this allows the fuel time to penetrate and mix with the coolant. For the LWR system, the fuel (UO_2, ZrO_2, steel) and

---

[6] D. E. MITCHELL, M. L. CORRADINI, and W. W. TARBELL, "Intermediate Scale Steam Explosion Phenomena: Experiments and Analysis," SAND 81-0124, Sandia National Laboratories (1981).

[7] M. BERMAN, "Light Water Reactor Safety Research Program Semi-Annual Report, October 1981-March 1982," SAND 82-1572, NUREG/CR-2841 (to be published).

[8] H. K. FAUSKE, "Some Aspects of Liquid-Liquid Heat Transfer and Explosive Boiling," *Proc. Fast Reactor Safety Mtg.*, Beverly Hills, California, April 2-4, 1974, CONF-740401, U.S. Atomic Energy Commission (1974).

[9] R. E. HENRY and H. K. FAUSKE, "Nucleation Characteristics in Physical Explosions," *Proc. Third Specialist Mtg. Sodium Fuel Interaction in Fast Reactors*, Tokyo, Japan, March 1976.

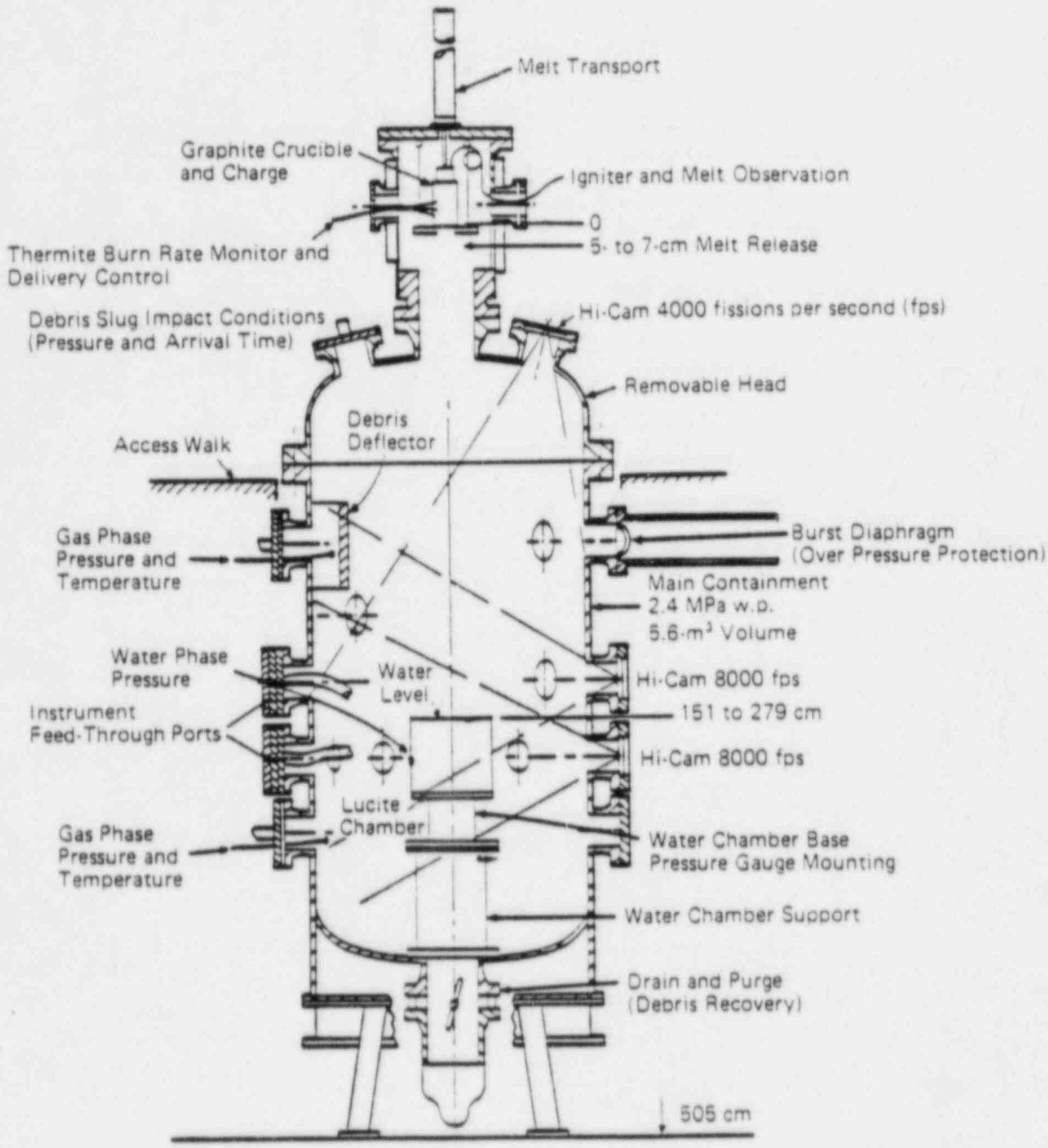

Fig. 1. The FITS containment chamber.

coolant (water) easily satisfy this first criterion (interface temperature calculated to be well in excess of the water critical temperature, 647 K). This criterion could be considered necessary but not sufficient.

Cho et al.[10] proposed that beyond this criterion, consideration must be given to the energy used in fuel-coolant mixing that creates more surface area and overcomes frictional effects. He concluded that frictional effects dominate the mixing process and developed a simple model to estimate the minimum required energy, E_m, for progressive mixing of the fuel and coolant:

$$E_m = 1.81\rho_m F_f\left(\frac{V_f^{2/3}}{t_b^2}\right)\left(1 - \frac{D_{FR}^2}{4V_f^{2/3}}\right)\ln\left(\frac{2V_f^{1/3}}{D_{FR}}\right) . \quad (1)$$

(A Nomenclature appears on p. xxx.) Using this approximate model, the energy required for fuel-coolant mixing can be calculated and compared to that available as thermal energy in the fuel, E_{th}. If E_m is

[10] D. H. CHO et al., "Mixing Considerations for Large-Mass, Energetic Fuel-Coolant Interactions," *Proc. ANS/ENS Fast Reactor Safety Mtg.*, Chicago, Illinois, October 5-8, 1976, CONF-761001, American Nuclear Society (1976).

substantially less than E_{fth}, then it indicates that mixing is possible from an energy standpoint.

Recently, Henry and Fauske[11,12] proposed a simple model to predict the minimum fuel diameter possible during fuel-coolant mixing. They base this model on the physical concept that the fuel can break up and remix with the water to a uniform size no smaller than that which would prevent liquid from entering the mixture zone; i.e., the fuel surface area increases (diameter decreases) to such a degree that steam generation stops liquid water inflow. To determine this minimum diameter, D_{min}, they equate the energy transferred from fuel to coolant in the mixture to the critical heat flux (CHF) in pool boiling (q''_{CHF}) multiplied by the cross-sectional area of the coolant. The CHF was viewed as an approximate hydrodynamic limit for steam outflow and water inflow (one-dimensional, counterflow, steady state). The minimum diameter is given by

$$D_{min} = \frac{6 m_f q''_{drop}}{\rho_f A_c q''_{CHF}} \quad , \tag{2}$$

where

$$q''_{drop} = \sigma_r (T_f^4 - T_c^4) + h_{film}(T_f - T_c) \quad . \tag{3}$$

Again this model can be viewed as an approximate physical limit. This physical model is geometrically approximate in two important respects: It assumes that the critical limit is reached in a planar surface neglecting transient effects, and it assumes that a counterflow of water and steam occurs, neglecting the possibility of steam outflow from one surface and water inflow from another surface (multidimensional effects). These omissions cause the model to neglect important effects. Mixing is not a static process occurring regardless of time; rather, it is a dynamic process always occurring to some degree, allowing the fuel to fragment to smaller and smaller sizes. For example, in the model by Henry and Fauske [Eq. (2)], the cross-sectional area of the chamber, A_c, should be replaced by the time-varying surface area of the fuel-coolant mixture. This would be the proper area for applying this flooding limit. Disregarding this concept might prompt one to seek strict limits to mixing, which are time independent; rather, the physics seem to suggest such limits are highly time dependent.

During the FCI, the approximate rate of fragmentation and the final debris size is empirically known from small- and intermediate-scale experiments.[6,7,13] These experiments indicate that the fuel fragments quickly (100 to 300 μs) to small sizes (from 1- to 10-mm to 50- to 150-μm mass average). Knowing the empirical debris size distribution, one can calculate the available surface area.

Recent Mixing Data

During a severe accident, fuel-coolant contact can occur in one of two ways: The fuel can pour into a water-filled cavity by gravity (or under pressure), or the water can reflood a cavity containing molten fuel. In the former case, the fuel falls through a coolant and mixes with it. In the latter case, the fuel is stratified with the coolant on top, and a slow quenching is the most probable result. In regard to fuel-coolant mixing, the former contact mode is of greater concern because of the possibility of a steam explosion during the mixing process. The stratified contact mode could also produce steam explosions, but the mixing would probably be limited by the initial density stratification.

This drop (pouring) contact mode was used extensively in FCI tests at SNL (Refs. 6, 7, 13, 14, and 15). In these tests, the hot fuel enters the water pool in film boiling and begins to distort in shape. As it continues to fall through the pool, it breaks apart into smaller pieces and mixes with the surrounding water while still in film boiling. These smaller pieces may subdivide further as the steam produced in film boiling flows out through the top of the fuel-coolant mixture and escapes the pool as water flows in from the sides. The mixture grows radially as the fuel, now mixed with water and steam, continues to fall through the pool, finally reaching the chamber base. Usually, one of two possible events occurs: An energetic FCI (steam explosion) is triggered, or the premixed molten fuel settles on the chamber base, reagglomerates, and eventually quenches. During this transient fall phase of the fuel through the water pool, one reason for breakup is inertial forces generated by the fuel initial relative velocity v_f and differences in density (ρ_f to ρ_c). If the fuel mass is large (characteristic diameter D_f large), or its relative velocity high, its characteristic Weber

[11] R. E. HENRY and H. K. FAUSKE, "Core Melt Progression and the Attainment of a Permanently Coolable State," *Proc. Mtg. Thermal Reactor Fuels* (Topl. Mtg. Reactor Safety Aspects of Fuel Behavior), Sun Valley, Idaho, August 2-6, 1981, American Nuclear Society (1981).

[12] R. E. HENRY and H. K. FAUSKE, "Required Initial Conditions for Energetic Steam Explosions," *Fuel-Coolant Interactions*, HTD-V19, American Society of Mechanical Engineers, Washington, D.C. (1981).

[13] M. BERMAN, "Light Water Reactor Safety Quarterly," SAND 80-1304, Sandia National Laboratories: Jan.-March, 1 of 4 (1980); April-June, 2 of 4 (1980); July-Sep., 3 of 4 (1981); Oct.-Dec., 4 of 4 (1981).

[14] L. D. BUXTON, W. B. BENEDICK, and M. L. CORRADINI, "Steam Explosion Efficiency Studies: Part II—Corium Experiments," SAND 80-1234, NUREG/CR-1746, Sandia National Laboratories (1980).

[15] L. D. BUXTON and W. B. BENEDICK, "Steam Explosion Efficiency Studies," SAND 79-1399, NUREG/CR-0947, Sandia National Laboratories (1980).

number (ratio of destabilizing inertial force $\rho_c v_f^2$ to stabilizing surface tension force σ/D_f) will be greater than a critical value ($We_{crit} = 7$ to 12 for relatively inviscid fluids[16]). The fuel will begin to distort and break apart.

One could develop an empirical model for this mixing phenomenon, if the assumption is made that hydrodynamic forces are the major cause of fuel-coolant mixing as in the case of isothermal experiments.[17-21] The major difference in these FCI experiments is that film boiling separates the two liquids; one might presume that the film acts like a low impedance fluid that delays the fuel breakup relative to the isothermal case. The dependent variables would be the depth of the fuel-coolant mixture H_m, the lateral dispersion diameter of the fuel-coolant mixture D_m, the mixture volume V_m, the displaced water volume V_D (i.e., the fuel and steam volume in the mixture at a given time), and the average fuel diameter during mixture D_{FR}. The independent variables are the fuel mass m_f, its diameter D_f, initial entry velocity V_f, coolant mass m_c, its depth H_c and width W_c properties, and time t.

To nondimensionalize the dependent variables, one can choose the fuel diameter, similar to hydrodynamic analysis[17-19]; the resultant groups are H_m/D_f, D_m/D_f, D_{FR}/D_f, V_m/V_f, and V_D/V_f, where V_f is the initial fuel volume $[V_f = (\pi/6)(D_f)^3]$. The independent variable, time, can be nondimensionalized by a characteristic time for hydrodynamic breakup τ_B. This time τ_B can be derived if one postulates what the mechanism for mixing is. Consistent with past analyses of hydrodynamic breakup,[20] we consider fuel breakup during this phase of the FCI to be controlled by Rayleigh-Taylor instabilities. In particular, τ_B is given by

$$\tau_B \sim D_f/v_B \ , \tag{4}$$

[16] J. O. HINZE, *AIChE J.*, **1**, 3 (1981).

[17] R. BENZ et al., "Hydrodynamic Analysis of Shock-Wave Induced Fragmentation in Liquid-Liquid Systems (Part I)," *Proc. 4th Committee on Safety of Nuclear Installations Specialist's Mtg. Fuel-Coolant Interactions in Nuclear Reactor Safety*, Bournemouth, England (Apr. 1979).

[18] M. BAINES and N. E. BUTTERY, RD/B/N3497, U.K. Central Electricity Generating Board, Berkely Nuclear Laboratory (1975).

[19] T. G. THEOFANOUS, "Fuel-Coolant Interactions and Hydrodynamic Fragmentation," *Proc. Fast Reactor Safety Mtg.*, Seattle, Washington, August 19-23, 1979, American Nuclear Society (1979).

[20] M. PILCH, "Acceleration Induced Fragmentation of Liquid Drops," Doctoral Thesis, University of Virginia (1981).

[21] M. PILCH and C. A. ERDMAN, *Trans. Am. Nucl. Soc.*, **38**, 403 (1981).

where v_B is the velocity of the Rayleigh-Taylor instability as it penetrates the fuel and subdivides it into smaller masses. Experiments in Rayleigh-Taylor instabilities[22] have indicated that shortly after the instability begins it reaches a constant velocity given by

$$v_B \sim (aD)^{1/2} + (a\lambda_m)^{1/2} \ , \tag{5}$$

where D is the length scale of the system (D_f in this case); λ is the fastest growing Taylor wavelength given by

$$\lambda_m = 2\pi\left[\frac{3\sigma_f}{a(\rho_f - \rho_c)}\right]^{1/2} \ ; \tag{6}$$

and where a is the acceleration. In this case, the acceleration is induced by the relative velocity between the fuel and the coolant:

$$a \sim \frac{3}{8}\frac{C_D}{D_f}\frac{\rho_c}{\rho_f}v_f^2 \ . \tag{7}$$

This penetration velocity appears to be composed of two parts: one due to the overall system length scale D_f, causing large wavelength instabilities to grow, and another due to the smaller fastest growing wavelength λ_m. For the phenomena considered here, it is not clear which component of the velocity is dominant.

To estimate τ_B and arrive at a dimensionless time, let us consider each component of v_B separately. If $v_{B_1} \sim (aD_f)^{1/2}$, then τ_B becomes

$$\tau_{B_1} = \frac{D_f}{v_f}\left(\frac{3}{8}C_D\frac{\rho_c}{\rho_f}\right)^{-1/2} \ , \tag{8}$$

where we have substituted for the acceleration from Eq. (7). The dimensionless time t/τ_{B_1} then becomes

$$\frac{t}{\tau_{B_1}} = \frac{tv_f}{D_f}\left(\frac{\rho_c}{\rho_f}\right)^{1/2} \ , \tag{9}$$

where $(\frac{3}{8}C_D)$ is approximately unity for liquid droplets. If $v_{B_{11}} \sim (a\lambda_m)^{1/2}$, then $t/\tau_{B_{11}}$ is given by

$$t/\tau_{B_{11}} = \frac{tv_f}{D_f}\left(\frac{\rho_c}{\rho_f}\right)^{1/2} We^{-1/4}\left(\frac{\rho_f}{\rho_f - \rho_c}\right)^{1/4} \ , \tag{10}$$

where

$$We \equiv \frac{\rho_c v_f^2 D_f}{\sigma_f} \ . \tag{11}$$

It is interesting to note that t/τ_{B_1} is the same dimensionless time T^*, used in empirical correlations for hydrodynamic droplet breakup, and $t/\tau_{B_{11}}$ is very similar in form to what Pilch derives for droplet breakup at a large Weber number.[20]

[22] M. L. CORRADINI, "Heat Transfer and Fluid Flow Aspects of Fuel-Coolant Interactions," PhD Thesis, Massachusetts Institute of Technology (1978).

TABLE I

Fuel Fragment Size Data During Mixing for FITS Experiments

FITS Test	Molten Fuel[a]		Entry Velocity (m/s)	Coolant Depth (m)	Time to Base Contact, t (ms)	Mass of Average Fuel Fragment Size-Base Contact	
	Composition	Mass (kg)				Visual[b] (mm)	Posttest[b] (mm)
MD-8	Iron alumina	4.7	6.4	0.71	180	8	Explosion
MD-11	Iron alumina	4.7	4.2	0.71	162	8	Explosion
MD-12	Iron alumina	1.46	5.3	0.457	135	8	Explosion
MD-15	Iron alumina	1.88	4.6	0.43	121	7	Explosion
MD-16	Iron alumina	1.85	5.4	0.43	121	7	Explosion
MD-18	Iron alumina	2.74	5.1	0.535	146	9	Explosion
MD-19	Iron alumina	5.1	5.9	0.61	172	7	Explosion
MDC-2	Corium	4.1	6.0	0.53	150	11	Explosion
MDC-16	Corium	8.5	6.0	0.53	140	12	Explosion
FITS-1A	Iron alumina	1.95	6.2	0.43	115	7	2 (partial interaction)
FITS-4A	Iron alumina	4.3	7.0	0.61	140	7	4 (partial interaction)

[a]Fuel was either iron alumina (Fe-55 wt%, Al_2O_3-4 wt%) or corium (UO_2-53 wt%, ZrO_2-17 wt%, stainless steel-30 wt%).

[b]Visual data based on camera speed of 2000 to 9000 fps and posttest mixing debris are not obtained when there is an explosion.

In the FITS experiments, a wide range of conditions was investigated using molten iron alumina and Corium as the fuel. The experiments analyzed for their mixing behavior are listed in Table I; the dimensionless time ranged from $0 < T^+ < 5$, and characteristic Weber numbers of $1000 < \mathrm{We} < 10\,000$. In all of the experiments performed, the width of the water chamber was large compared to fuel diameter; subsequent FITS tests investigate this parameter.

The mixing data from some of the FITS experiments are plotted as a function of $t/\tau_{B_1}(T^+)$ in Figs. 2, 3, and 4. Mixture properties are used for the metal-oxide fuel in these calculations. First, note that the data follow similar trends for the range of experiments performed to date ($1 < m_f < 20$ kg). If one plots the same data as a function of the other dimensionless time $t/\tau_{B_{11}}$, the same trends are observed (Figs. 5 and 6). Subsequent experiments might be performed at larger scales to determine if these dimensionless groups can still successfully correlate the data.

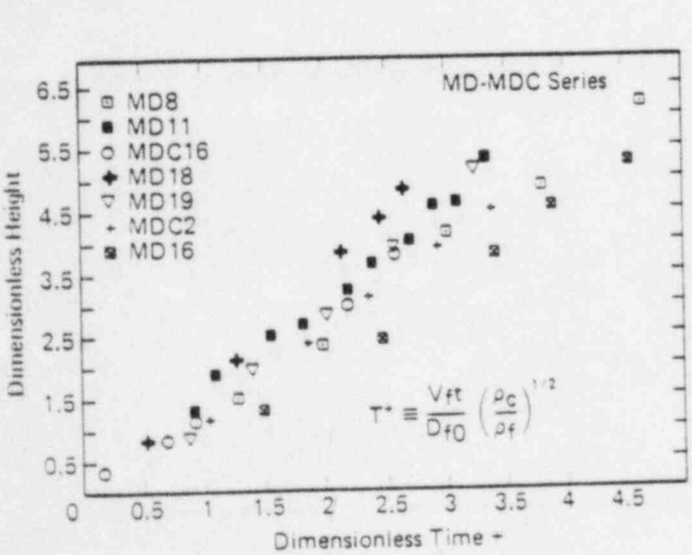

Fig. 2. Correlation of FITS mixing data, height versus time.

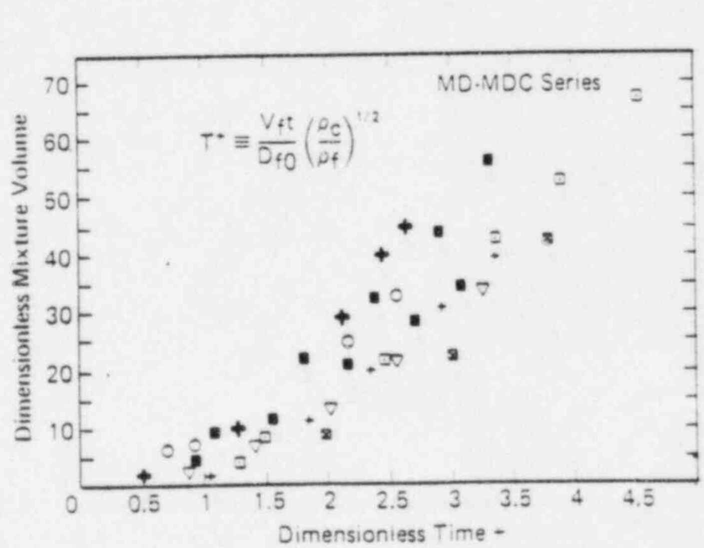

Fig. 3. Correlation of FITS mixing data, mixture volume versus time.

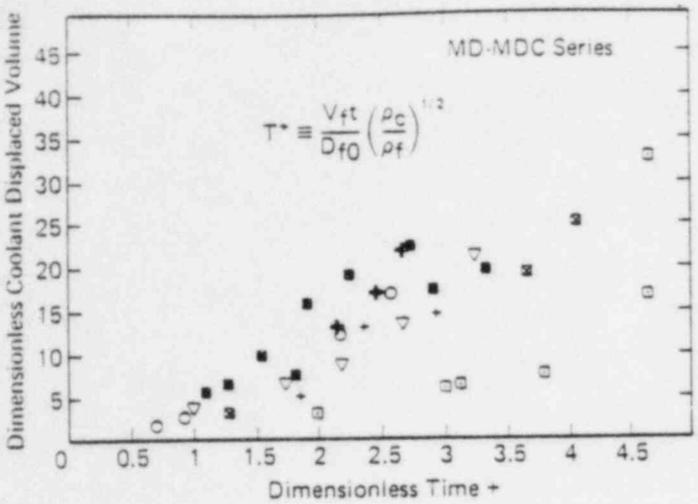

Fig. 4. Correlation of FITS mixing data, coolant displaced volume versus time.

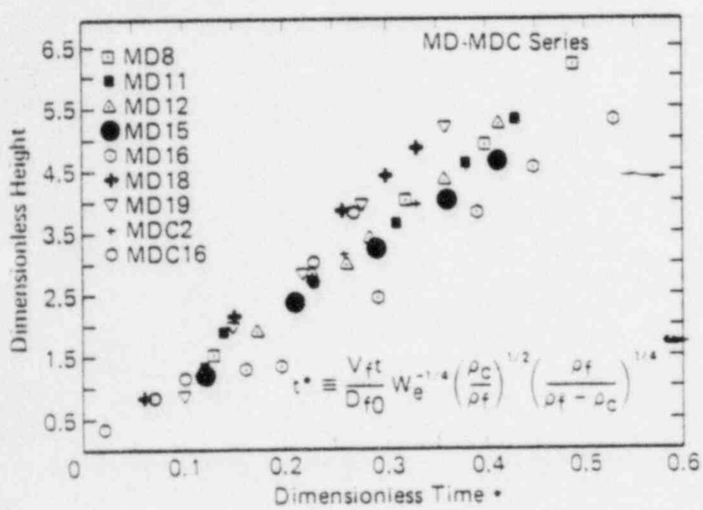

Fig. 5. Correlation of FITS mixing data, height versus time.

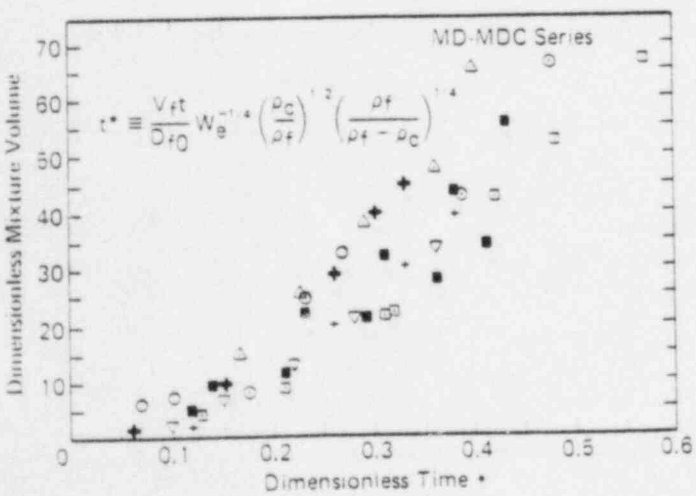

Fig. 6. Correlation of FITS mixing data, mixture volume versus time.

or what other groupings are appropriate. In particular, the fuel fragment diameter, the mixture volume, and displaced water volume are important, since they determine the fuel surface area and the average volume fraction of fuel and steam. Knowing these quantities would aid in predicting steam and hydrogen generation rates.

Finally, if one compares the trends of H_m/D_f and D_m/D_f for these FITS data with previous data from isothermal tests, one finds that the rate of growth of the fuel coolant mixture in FITS is slower for a given time than for isothermal tests. This seems to suggest that the steam generated in these tests adds compliance to the fuel-coolant system and slows fuel-coolant mixing over a given time span.

The data for the observed fuel fragment size D_{FR}/D_f are not plotted, but are tabulated in Table I. This is because the visual data could only be obtained at the end of the test near base contact when the fuel-coolant mixture was large and the fuel droplets could be individually measured. It is recognized that visual measurement of fragment sizes is prone to larger errors. The diameter measured may be larger than the actual diameter due to the luminous image the drop creates on the film; the posttest debris data bear this observation out for two other FITS experiments (FITS 1A and 4A).

The previous correlation of test data applies as the fuel falls through the coolant. If the coolant chamber is narrow and its depth shallow, mixing during the fall phase would be impeded or stopped. Also, the effect of structure on the mixing process is not known. Mixing on the chamber bottom would probably not be very efficient. Current FITS data indicate in the absence of an explosion that the melt falls to the base and reagglomerates as it quenches. There are no definitive data to indicate how effective the fuel-coolant mixing is on the chamber base.

Limits to Fuel-Coolant Mixing

If the steam generation rate becomes too large as the fuel and coolant mix the fuel (or coolant) could be rapidly carried out (fluidized) of the mixture and mixing would be impeded. It is important that one identifies these physical limits to mixing because they represent the bounds that would be set on this dynamic process.

The effect of the physical boundaries is qualitatively obvious, although not quantitatively known. Base contact would most likely trigger an energetic FCI (steam explosion) as the FITS data indicate. If not, the fuel settles on the chamber base and slowly quenches. However, in the accident the decay heat power combined with the fuel molten state may cause prolonged thermal attack of concrete basemat. The gases generated by this concrete decomposition would

bubble through the fuel and may enhance fuel-coolant mixing in this stratified geometry.

Limits on fuel-coolant mixing due to steam generation could cause the fuel (or coolant) to be carried away with the steam flow. One would expect the mixing process to be self-limiting; i.e., given sufficient time, the fuel would mix and break up to an average size no smaller than that which would cause the liquids to be fluidized and swept away. The fuel droplet distribution and the average diameter D_{FR} may be larger than this limit if time is short (due to a small water depth or a triggered explosion). In addition, because the fuel enters the water in a pouring mode of contact, the mass first to reach the coolant chamber bottom would be better mixed than fuel at the top of the water pool. Therefore, if one were to identify this limit on mixing, it would represent the minimum average fuel diameter to which all the fuel falling through the coolant could fragment before the mixture would begin to be fluidized.

To find this minimum fuel diameter D_{FR} for the case of fluidization of the fuel droplets, one would equate the velocity needed to fluidize a particle v_{FL} to the steam velocity v_v at any location in the fuel-coolant mixture caused by fuel-coolant heat transfer. Based on a steady-state momentum balance, the fluidization velocity for a single droplet is given by

$$v_{FL} = \left[\frac{4}{3}\,\frac{D_{FR_1} g}{C_D}(\rho_f/\rho_v)\right]^{1/2} , \tag{12}$$

where ρ_v is the steam density, g is the gravitational acceleration, and C_D is the drag coefficient, corrected for the effect of an array of droplets[23,24] ($C_D \sim 1$). Now, the steam velocity cannot exceed this value or the fuel droplets will be swept away. This would first occur at the top of the mixture where all the steam from the whole mixing zone exits to maintain equal pressure with the ambient. Let us consider the steam velocity at the top of the mixture, realizing that the fuel droplet diameter determined from this simple analysis would signal the beginning of the fuel sweepout. Actually, the average fuel diameter in a test could fall slightly below this limit before a majority of the fuel begins to be swept away. The steam velocity at the top of the pool is found by an energy balance to be

$$v_{v_{top}} = \frac{\dot{m}_{v_{top}}}{\rho_v A_m \alpha_v} \tag{13}$$

[23] J. COLLIER, *Convective Boiling and Condensation*, 2nd ed., McGraw-Hill Book Company, Inc., New York (1981).

[24] G. WALLIS, *One-Dimensional Two-Phase Flow*, 2nd ed., Chap. 12, p. 378, McGraw-Hill Book Company, Inc., New York (1981).

$$\dot{m}_{v_{top}} = \frac{6\alpha_f V_m q''_{drop}}{D_{FR_1} i_{fg}} \tag{14}$$

$$q''_{drop} = \sigma_r(T_f^4 - T_{sat_c}^4) + h_{film}(T_f - T_{sat_c}) . \tag{15}$$

Note that all the energy transferred from the fuel to the coolant was assumed to go into producing steam primarily by black-body radiation. These assumptions neglect subcooling of the coolant and the reduction of the radiation view factor due to properties and radiation to other fuel particles. Also, the steam film separating the fuel drop from the water may absorb some amount of the radiative energy from the fuel. This would reduce fuel heat loss and the steam generation rate. While this effect would not be very important at the low pressures of the FITS tests, this would become very significant for the full-scale application where very high system pressures are possible ($\sim$170 bar). This may drastically reduce the steam generation rate and allow for mixing to a smaller fuel diameter. Finally, in estimating the radiative heat transfer, the average fuel droplet temperature T_f was used. The correct fuel temperature to be used should be the surface temperature of the fuel drop, which would be lower due to the conduction resistance in the fuel droplet. This approximation also overestimates the radiation heat loss from the fuel and therefore overestimates the rate of steam generation. Although one may consider these second-order effects, all of them would reduce the effective heat flux from the drop, q''_{drop}, and reduce the predicted minimum mixing diameter (i.e., allow more mixing). When all of these terms are substituted back into Eq. (13), the result is

$$v_{v_{top}} = \left(\frac{\alpha_f}{\alpha_v}\right)\left(\frac{6q''_{drop}}{\rho_v i_{fg}}\right)\left(\frac{H_M}{D_{FR_1}}\right) , \tag{16}$$

where H_M is the mixture height. When the two velocities are equated, one gets for the average minimum mixing diameter

$$D_{FR_1} = \left(\frac{3}{4}\right)^{1/3}\left(\frac{\alpha_f}{\alpha_v}\right)^{2/3}\left(\frac{6q''_{drop}}{\rho_v i_{fg}}\right)^{2/3} \times \left(\frac{C_D H_M^2}{g}\right)^{1/3}\left(\frac{\rho_v}{\rho_f}\right)^{1/3} . \tag{17}$$

Remember that all the assumptions used to derive this simplified mixing diameter limit predict the threshold for fuel sweep out from the top of the mixture. Average fuel sizes could fall slightly below this limit before a major fraction of the fuel would begin to be fluidized. For example, if one equated these velocities near the bottom of the mixture (e.g., the lower third of V_m) to assure a majority of the fuel would be swept out the predicted D_{FR_1} would decrease by a factor of 2. Also, realize that this is a quasi-steady limit and applied only insofar as one

knows the mixing zone conditions (i.e., volume fractions in mixing zone at a given time as calculated from Figs. 2 and 3) at any point in time. The empirical correlations developed from FITS tests that were just presented would give one the initial conditions needed to use this model.

Note that this physical limit is different from the model proposed by Henry and Fauske.[9,11] In this model, the physical picture is that the steam flows out the top of the fuel-coolant mixture, water flows in from the bottom and sides, and the fuel falls and disperses radially. This picture is more in line with the debris bed sweepout concepts put forth by Rivard et al.[25]

To find the minimum fuel diameter for the case of fluidization of the coolant that enters the mixing zone, $D_{FR_{II}}$, one would perform the same analysis as before, except the fluidization velocity is based on the coolant length scale D_c. If one assumes that the

$$v_{FL} = \frac{4}{3}\left(\frac{D_c g}{C_D}\right)(\rho_c/\rho_v)^{1/2} \tag{18}$$

ratio of the coolant volume surrounding a fuel droplet to the fuel drop volume is proportional to the ratio of the total coolant volume to the fuel volume in the mixing zone, the result is

$$\frac{D_c^3}{D_{FR_{II}}^3} - \frac{\alpha_c V_M}{\alpha_f V_M} , \tag{19}$$

where α_c is the coolant volume fraction in the mixture. This gives a relation between D_c and $D_{FR_{II}}$:

$$D_c = D_{FR_{II}}(\alpha_c/\alpha_f)^{1/3} . \tag{20}$$

The result in combination with Eqs. (9) and (13) gives and estimate of $D_{FR_{II}}$:

$$D_{FR_{II}} = \left(\frac{3}{4}\right)^{1/3}\left(\frac{\alpha_f}{\alpha_c}\right)^{2/9}\left(\frac{\alpha_f}{\alpha_v}\right)^{2/3}\left(\frac{6q''_{\mathrm{drop}}}{v^i fg}\right)^{2/3} \times\left(\frac{C_d H_M^2}{g}\right)^{1/3}\left(\frac{\rho_v}{\rho_c}\right)^{1/3} . \tag{21}$$

The same comments concerning D_{FR_I} are applicable here; the volume fractions of fuel and steam are needed from the experiments or separate analysis to employ this model.

A prediction of the minimum fuel mixing diameter due to fluidization can be made using Eqs. (17) and (21). These calculations could be compared to the actual data of D_{FR} (Table I) to determine if the model is in agreement with the observed data. The results of the calculation are presented in Table II, and the agreement between the model and the data is good. The agreement between the proposed mixing limit and the data also suggests that the fall time was sufficiently long ($2.5 < T^+ < 5$) to allow the fuel to break apart to a small diameter. One could use this criterion of dimensionless time to predict the mixing time and minimum diameter for larger scale FCI events.

Note that in all the tests the fuel mass was a mixture of an oxidic phase (UO_2-ZrO_2 or Al_2O_3) and a metallic phase (stainless steel or iron). In the calculation, it was assumed that the heterogeneous mixture behaved as a homogeneous fuel with average mixture

[25] J. B. RIVARD et al., "Report of the Zion/Indian Point Study," SAND 80-0617/1, NUREG/CR-1410, Chap. 6, Vol. 1, Sandia National Laboratories (1980).

TABLE II

Prediction of FITS Mixing Behavior

(Calculations are based on volume fractions from FITS data and measured fuel temperatures of ~2700 K.)

FITS Tests	Time to Base Contact $T^+ = t/\tau_{B_I}$	Minimum Mixing Diameter		Maximum Steam Generation Rate		Maximum Hydrogen Generation Rate	
		D_{FR_I} (mm)	$D_{FR_{II}}$ (mm)	D_{FR_I} (g·mol/s)	$D_{FR_{II}}$ (g·mol/s)	D_{FR_I} (g·mol/s)	$D_{FR_{II}}$ (g·mol/s)
MD-8	4.33	6.5	8.3	101	79	2.2	1.7
MD-11	2.61	8.3	10.4	79	63	1.7	1.3
MD-12	3.88	7.1	9.5	40	32	0.98	0.79
MD-15	2.78	6.3	8.2	33	26	0.88	0.66
MD-16	2.53	6.3	8.2	33	25	0.88	0.66
MD-18	3.36	7.2	9.7	39	31	1.04	0.81
MD-19	3.72	7.0	8.9	81	64	2.2	1.7
MDC-2	3.26	6.0	12.1	76	38	2.0	1.0
MDC-16	2.61	6.0	12.1	156	78	4.2	2.1
FITS-1A	3.56	5.8	7.3	47	37	0.98	0.77
FITS-4A	3.56	7.3	9.3	82	65	1.8	1.4

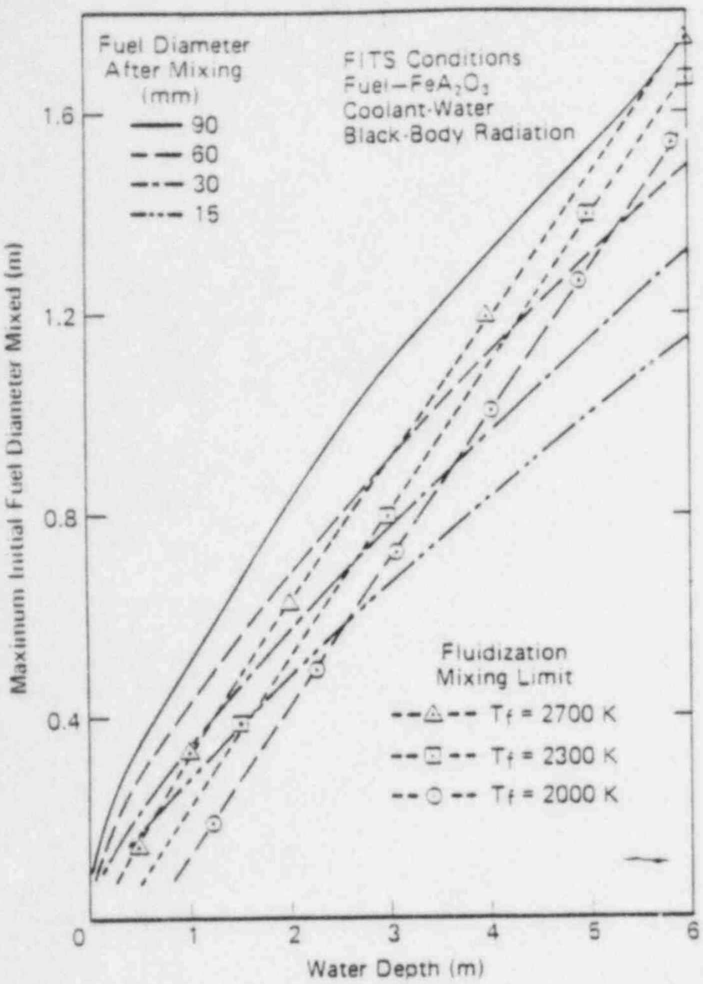

Fig. 7. Limits to fuel-coolant mixing.

properties. This is a reasonable first approximation based on the data,[26] indicating that posttest debris was compositionally homogeneous for any diameter range. Note also that the minimum energy required for mixing, E_{Vf} [Eq. (1)], is very small—5 to 10 J; this is <0.1% of the fuel thermal energy.

One could generalize this concept of a limit to mixing for fuel-coolant masses. Because the mixing process is dynamic, the characteristic diameter of the fuel mass in the water pool is bounded by its initial diameter D_{f0} (assuming a single spherical mass), when it enters, and its diameter at the fluidization limit D_{FR_I} or $D_{FR_{II}}$, when it has fallen through a sufficient depth of water after some time. The diameter of the fuel at a time between these could be approximated by a simple transient model as used in hydrodynamic droplet breakup[18] {e.g., $D_f = D_{f0}[\exp(-T^*)]$}. One then realizes that the important variable is not time but the product of the fuel velocity and time, i.e., the depth through which the fuel has traveled. One can combine this concept with the limit to mixing to predict the maximum mass of fuel that could mix for a given water depth ($v_f t$), and the final diameter of the fuel (see Fig. 7). In this figure, the fuel diameter after mixing is given for a specific depth, $H_c = v_f t$, and initial fuel diameter, D_{f0}. We also plot the fluidization limit, D_{FR_I}, for different fuel temperatures assuming black-body radiation. All the fuel diameters after mixing to the left of the fluidization limit for a given fuel temperature can mix, while those mixing diameters to the right of the limit for a given H_c and D_{f0} will begin to fluidize. Note that as H_c increases, the minimum diameter for mixing (given by the intersection of a fuel mixing diameter curve and the fluidization limit for a given fuel temperature) increases significantly.

Steam/Hydrogen Generation

Assuming that one now can estimate the minimum fuel diameter during mixing and therefore calculate the maximum fuel surface area, steam and hydrogen generation rates could be determined. The rate of steam generation is found by multiplying the heat flux from one drop q''_{drop} [Eq. (12)] by the heat transfer area and dividing it by the energy necessary to vaporize the water [$i'_{fg} = i_{fg} + c_{Pc}(T_{sat} - T_c)$]; the result is

$$\dot{m}_v = \left(\frac{6m_f}{{}_f D_{FR}}\right)\frac{q''_{drop}}{i'_{fg}} . \tag{22}$$

If one uses the minimum mixing diameter, the resulting steam generation rate is a maximum. Numerical results are presented in Table II for the FITS tests.

The kinetic rate of metal oxidation and hydrogen generation is a function of three important variables: the temperature of the fuel surface at which oxidation is occurring, the rate of diffusion of the vapor to the fuel surface, and the rate of diffusion of the oxygen into the liquid phase. Currently, there are no experimental data available to determine the rate of reaction of water with molten metallic reactor materials (zirconium or stainless steel). It is expected that this reaction rate also would be controlled by mass transfer in the liquid fuel phase given an abundance of steam. In certain zirconium-water experiments, Baker and others[26-29] approximated the molten reaction rate in

[26] G. F. LIEN, Ed., *Superheater Alloys in High Temperature High Pressure Steam*, American Society of Mechanical Engineers, New York (1968).

[27] L. BAKER and L. C. JUST, "Studies of Metal-Water Reactions at High Temperatures. III Experimental and Theoretical Studies of the Zirconium-Water Reaction," ANL-6548, Argonne National Laboratory (May 1962).

[28] J. V. CATHCART et al., "Zirconium Metal-Water Oxidation Kinetics IV. Reaction Rate Studies," ORNL/NUREG-17, Oak Ridge National Laboratory (Aug. 1977).

[29] J. T. BITTLE et al., *Corrosion NACE*, **25**, *1* (1969).

calculations by assuming mass transfer in the gaseous phase (steam diffusion) was the limiting process. If one uses this assumption, the metallic fuel droplet can be modeled to be in a quasi-steady oxidation process. The governing mass transfer equation[30] can be written in spherical coordinates and integrated to give the molar hydrogen generation rate for the droplet

$$\dot{N}_{H_2} = \frac{4\pi D_0 P_{H_2}}{R_0 T_v}\left(\frac{1}{R_{FR}} - \frac{1}{R_C}\right)^{-1} , \tag{23}$$

where R_c is the radius of vapor-liquid coolant interface. Based on small-scale FCI tests,[11] the vapor film thickness is on the order of 1 mm when hydrogen is present. The total generation rate is found by multiplying the rate per droplet by the total number of droplets (the total metallic fuel mass divided by the mass of a droplet).

Using the minimum mixing diameters, the maximum hydrogen generation rate was calculated and is given in Table II. Note that the rate of hydrogen production is ~50 times smaller than that for steam. In fact, if one uses this maximum generation rate with the mixing time in the FITS experiments, only a few grams per mole of hydrogen are predicted to be produced. This corresponds to ~5% of the total metallic mass reacted.

STEAM EXPLOSIONS

Triggering and Propagation

In Refs. 28 and 31, we described the steam explosion process and divided it into four separate phases—mixing, triggering, propagation, and expansion. The recent FITS experiments, which we discuss here, showed that these phases were still distinct, but that triggering and propagation are more complicated than was first reported in Ref. 6.

As opposed to the more common base triggering phenomena observed in those experiments that only used 2 to 5 kg of melt, we observed triggers that occurred randomly—at or near the water surface, at or near the water chamber base or side walls, and on occasion at all of these locations. Some of these triggers escalated into propagating wave through the melt-water mixture, while the remainder decayed locally with no continuing observable effect. When recorded by the cameras, triggers appeared as rather complicated wave-like phenomena in the water surrounding the melt-water mixture. Propagation had a similar appearance, but occurred in the melt-water mixture and resulted in significant extinction of melt luminosity.

Table III describes the nine experiments conducted in the FITSB series, and a description of some of the important features is discussed below. The table also includes data from the other in-chamber tests (FITS A and G series).

Experiments 2B, 3B, 7B, and 9B all resulted in single explosions, triggered either at the water surface or water chamber base. The sequence of events leading to these explosions was similar to the earlier 2- to 5-kg experiments. Immediately after contact with the water, the melt at the periphery of the mixture was observed to fragment into droplets estimated to be between 10 and 20 mm in diameter. The fragmentation and mixing continued until the time of explosion trigger. Chamber air pressure records for these single explosions showed three characteristic features, which depended on initial conditions such as water depth and mass ratio. These characteristics were a short rise time to the pressure peak, a relaxation in ~20 ms to a quasi-static plateau, and late-time chamber repressurization due to steam generation with possible augmentation by hydrogen production.

Figure 8 for FITS7B, at a mass ratio of 1.5:1, shows essentially no steam explosion peak, but a large steam generation pressure rise followed by what might have been a hydrogen combustion event. By contrast, Fig. 9 for FITS9B, at a mass ratio of 9:1, shows a significant steam explosion pressure peak and associated pressure plateau followed by a modest steam generation pressure rise.

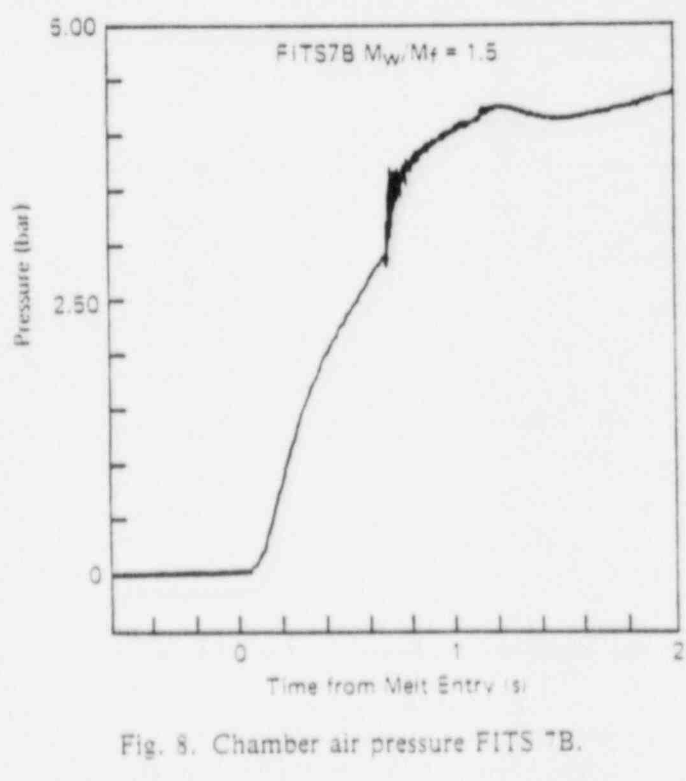

Fig. 8. Chamber air pressure FITS 7B.

[30] R. B. BIRD et al., *Transport Phenomena*, John Wiley and Sons, Inc., New York (1960).

[31] M. L. CORRADINI, *Nucl. Sci. Eng.*, **82**, 429 (1982).

TABLE

FITS Initial Conditions

Experiment	Melt			Water		
	Mass (kg)	Entry Volume (m/s)	Average Diameter at Entry[a] (cm)	Geometry Square × Deep (cm)	Mass (kg)	Temperature (°C)
1A	1.94	6.2	3.5	46 × 43	90	10
2A	2.87	4.6	3.6	53 × 53	152	13
3A	5.3	5.0	3.3	61 × 61	226	24
4A	4.3	7.0	3.5	61 × 61	226	25
5A	5.4	5.3	3.2	61 × 61	226	24
1B	18.7	5.4	4.1	61 × 61	226	25
2B	18.6	6.0	6.0	61 × 30	113	25
3B	18.6	6.0	24.0	43 × 30	57	22
4B	18.7	6.8	5.8	61 × 61	226	26
6B	18.7	7.2	6.5	46 × 30	63.4	94
7B	18.7	7.4	Not observed	43 × 15.2	28.1	18
8B	18.7	6.5	29.0	61 × 76	283.5	15
9B	18.7	7.0	5.6	61 × 45.7	170.0	16
1G	20.4	8.0	Dispersed	61 × 2	44	94
2G	13.5	8.0	Dispersed	61 × 54	110	94

[a]Optical measurement.
[b]Melt density = 3.8 g/cm^3.

Three of the experiments (FITS 1B, 4B, and 8B, see Table III), having mass ratios of 12, 12, and 15 and water depths of 61, 61, and 76 cm, respectively, resulted in double explosions; i.e., there were two explosive interactions separated by ~120 to 140 ms in each experiment.

The first explosion in FITS1B occurred 142 ms after melt entry and was similar to the single explosions described above. It was estimated that 14 kg of the total of 18.7 kg of melt was coarsely mixed in the water prior to triggering of the explosion at the melt-water interface on or near the water surface. The explosion was triggered before the submerged leading edge of the melt had contacted the water chamber base, and the direction of propagation was downward at ~300 m/s. Pieces of water chamber and residual water and melt impacted the camera ports before the second explosion, which was not immediately observed; this explosion only became apparent when active pressure data became available. Comparison of active data and visual observations showed that there was a second explosion 133 ms after the first. Chamber air pressure data (Fig. 10) showed two peaks due to the steam explosions and two corresponding pressure plateaus, followed by a small late-time repressurization. FITS4B and 8B were attempted to reproduce the FITS1B double explosion result and to determine if entry velocity and/or water depth were important initial conditions for a double explosion; the results, however, were not qualitatively different from FITS1B. Only a small quantity of melt was in the water prior to a surface-triggered first explosion (~1.7

III
and Observations

Initial Ratio Water Melt		Spontaneous Expolsion		
Mass	Volume	Location	Time After Melt Entry (ms)	Other Observations
46	178	Not observed	0.115	Mild interaction
53	203	Surface	0.075	Surface explosion
43	163	Below surface	0.150	Single explosion
53	201	Not observed	---	No spontaneous explosion at 1.1 MPa
43	163	Base triggered	0.25	Triggered explosion at 1.1 MPa
12.0	46.0	Surface Unknown	142 275	First explosion Second explosion
6.0	23.0	Surface	84	Single explosion
3.0	11.5	Base	77	Single explosion weak interaction at surface at 70 ms after entry that did not propagate
12.0	46.0	Surface Base	16 134	First explosion Second explosion
3.4	12.9	None	---	Multiple interactions at 40, 57, 82, and 153 ms after melt entry; no propagation or steam explosion
1.5	5.7	Not observed	80	No camera data, time estimated from water phase gauges
15.0	57.4	Surface Base	27 146	First explosion Second explosion
9.0	34.6	Base	98	Single explosion
2.0	7.6	---	---	No explosion occurred in either FITSG test due to high entry velocity and fuel predispersed fuel mass, quench times were 20 to 30 s
8.0	30.4	---	---	

kg in FITS4B and 1.9 kg in FITS8B). These explosions, although not recorded by the water phase transducer (~60 cm from the explosion site), were observed visually and were sufficiently energetic to cause the water chambers to fail; i.e., the walls and water began to move radially outward toward the camera ports.

Melt fragmentation and mixing in the residual water were enhanced by the first explosion. It was observed that the melt was fragmented more thoroughly: There were more droplets, and they were typically in the 5- to 10-mm-diam range. In addition, the melt was more dispersed, and its velocity, as it fell through the residual water, was approximately twice that observed when no explosion occurred. The second explosion occurred at approximately the time the melt-water mixture contacted the water chamber base. Due to the severe geometry distortion caused by the first explosion, a propagating wave was not visually observed in any of these second explosions.

In a steam explosion, some fraction of the internal energy of the fuel is transferred to the coolant and increases its internal energy during the triggering and propagation phase. The coolant then, having a large vapor pressure, expands against its inertial constraints and transforms some of its internal energy into kinetic and potential energy of the constituents involved in the explosion (fuel, water, air). If the explosion occurs in the open environment, then the explosion products expand down to one atmosphere. In the FITS experiments, in the containment chamber, some of the fuel internal energy eventually goes into compressing the

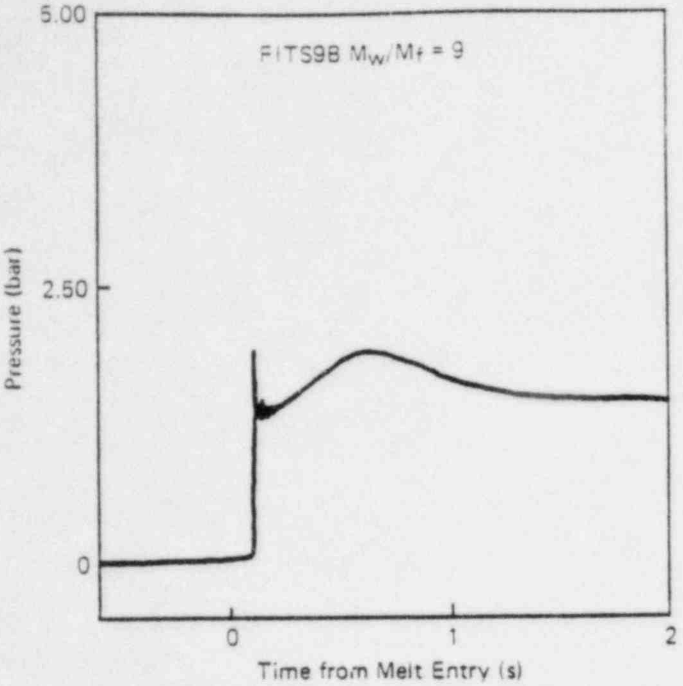

Fig. 9. Chamber air pressure FITS 9B.

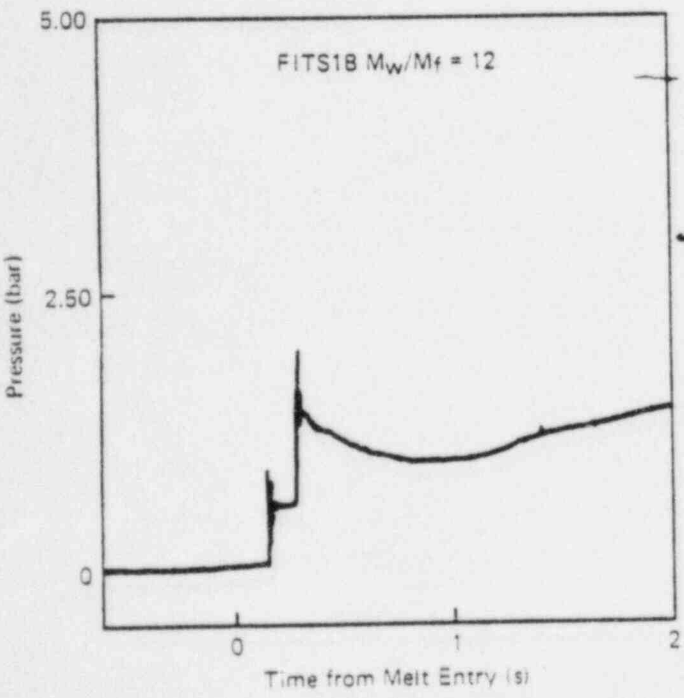

Fig. 10. Chamber air pressure FITS 1B.

chamber atmosphere (Fig. 11). Therefore, at any time after the steam explosion trigger in the FITS tests, the fuel internal energy appears principally in two forms—internal or kinetic energy of the constituents. The sum of these two quantities at any point in time (assuming adiabatic chamber walls) is a measure of the energy derived from the explosion, i.e., analogous to a heat of detonation from a chemical reaction. Different geometries and degrees of confinement can alter the partition of the energy between fuel and coolant, kinetic, and internal.

By measuring the dynamic pressure in the water phase, the impulse delivered to the base, and the velocity of the chamber walls during the early expansion phase, the peak kinetic energy of the explosion was calculated. Because of the difficulties in obtaining some of the data, these calculations are subject to errors of 10 to 30%. One ratio of interest then is this kinetic energy relative to the original fuel internal energy—sometimes called the explosion conversion ratio η_{KE}. The internal energy of the constituents at any point in time is a much more difficult quantity to measure. However, an estimate of it can be obtained by measuring the pressure rise in the FITS containment chamber.

Experimental Data Analysis

The mixing that occurs before the explosion is triggered should have an effect on the subsequent explosion. If ample time is given for the fuel to break up into smaller diameter droplets and disperse in the liquid coolant pool, more of the fuel mass will be able to rapidly fragment during the explosion into fine debris; this, in turn, will probably increase the explosion conversion ratio (ratio of the measured kinetic energy to the initial fuel thermal energy). This is empirically demonstrated for the FITS tests if one plots the explosion conversion ratio η_{KE} and the fuel debris diameter as a function of the initial coolant-to-fuel mass ratio (Fig. 12). In these tests, the fuel is dropped into the water as a coherent mass and triggered after mixing in the available water mass. Note that the conversion ratio rises to almost a constant value (1 to 2%) after the fuel-to-coolant mass ratio increases above 3

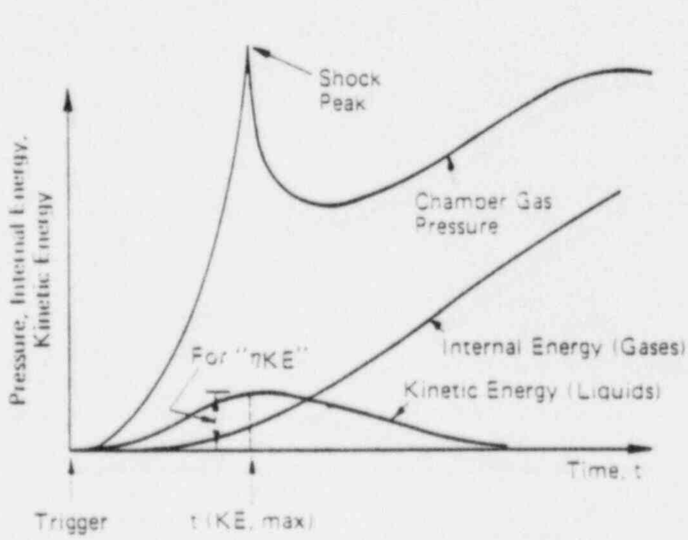

Fig. 11. Qualitative history of pressure and energy during the explosion.

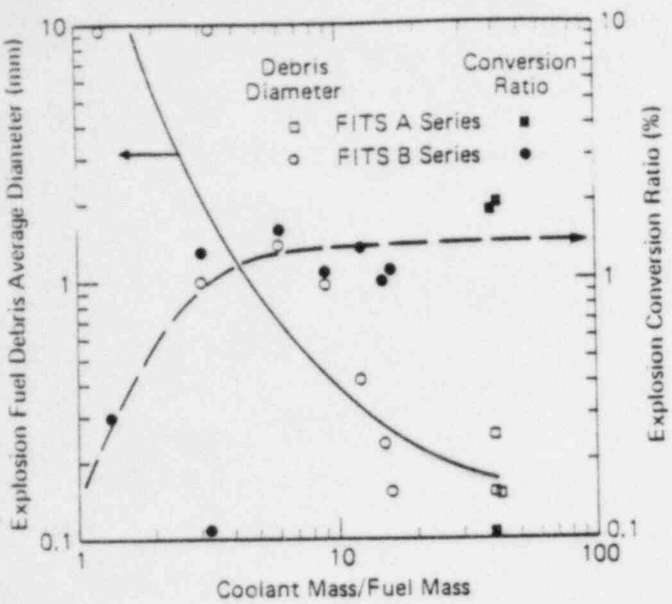

Fig. 12. Explosion conversion ratio and debris diameter as a function of coolant-to-fuel-mass ratio.

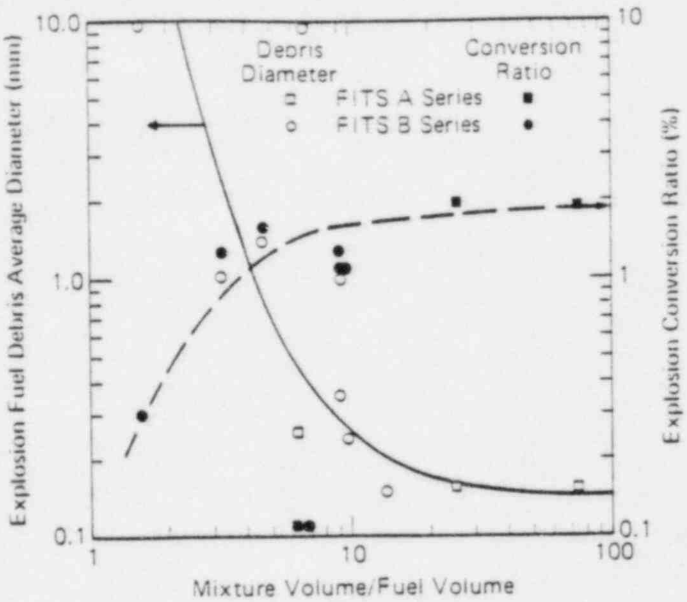

Fig. 13. Explosion conversion ratio and debris diameter as a function of mixture-to-fuel-volume ratio.

In contrast, the average fuel debris diameter continues to decrease in magnitude until the mass ratio becomes very large (20 to 1).

The same effect can be better observed if one plots the debris diameter and the conversion ratio as a function of the ratio of the fuel-coolant mixtures volumes at the time of the explosion to the original fuel volume V_m/V_f. The reasoning here is that as the mixture-to-fuel volume ratio increases, the fuel has more time to disperse in the coolant, break up into smaller sizes, and produce a more efficient explosion. Figure 13 indicates even more clearly the strong correlation of the explosion fuel debris size to initial mixing behavior. Again, one notes how the conversion ratio quickly rises to nearly constant values.

It is interesting to note that even when the fuel debris seems relatively coarse (~1 mm as in the FITSB series), the conversion ratio is still large, 1 to 2%. This suggests that the percentage of fuel "participating" in the explosion cannot be arbitrarily taken to be small (e.g., based on a thermal equilibration time during the explosion 200 m). Rather, even the "coarse" fuel debris probably participates in the explosion to the extent that it can transfer the thermal energy of its outer surface quickly, and therefore, can affect the explosion conversion ratio. These data suggest one must be careful when trying to distinguish between what fuel "mixed" with water and what fuel participated in the explosion. This is further illustrated if one computes the "Sauter-mean" diameter for the debris (see Table IV). This diameter is the correct average value to characterize the surface area to volume ratio of debris size distribution.[23,24] Note that for even the low efficiency FCIs (3B, 6B, and 9B), the Sauter-mean diameter is small, much smaller than the mass mean size. This again suggests that much of the fuel debris could become involved in the FCI.

CURRENT OBSERVATIONS AND CONCLUSIONS

The current FCI experiments conducted at SNL were analyzed to determine the fuel-coolant mixing behavior and the effect of mixing on the explosion energy and debris. Data were well correlated in terms of dimensionless groups derived from the concept that fuel mixing was governed by hydrodynamic breakup (i.e., Taylor instabilities). Physical limits to mixing were proposed, which indicate that the minimum mixing diameter is limited by fuel or liquid coolant fluidization, Eqs. (17) and (21). Using experimental values for steam volume fraction allowing us to predict with good agreement the fuel diameter after mixing had taken place. This mixing model was used to calculate the rate of hydrogen and steam generation in the FITS tests. Finally, the explosion data (η_{KE} and debris size) was noticeably affected by the fuel-coolant mixing process. The steam explosion experiments also show that the conversion ratio η_{KE} did not vary significantly with either mass ratio or water geometry with the exception of the extremely lean mass ratio (FITS7B). It is finally important to point out that multiple explosions occurred (~100 ms apart) when $12 < m_c/m_f < 15$; also, with these multiple events, it appeared that the first explosion enhanced the coarse mixing for the subsequent explosion.

TABLE IV

FITS Steam Explosion Results

Experiment	Initial Mass Ratio, M_c/M_f	Melt[a] Energy, Q_m (MJ)	Melt Mass Averaged Particle Size (μm)	Sauter-Mean Diameter (μm)	Conversion Ratio (%)
1A	46	5.43	2 000	2400	0.0
2A	53	8.04	260	176	1.0
3A	43	14.8	155	90	1.5
4A	53	12.04	3 800	4740	Small
5A	43	15.1	155	92	1.5
1B	16	39.2		188	1.1
	12	52.4	200		Not measured
2B	6	52.0	1 400	565	1.6
3B	3	52.0	1 100	330	1.3
4B	12	52.4	250	215	1.3
6B	3.5	52.4	10 000	2100	Small
7B	1.5	33.6	7 000	1190	0.3
8B	15	52.4	145	100	1.5
9B	9	52.4	900	326	1.1

[a]Based on 2.8 MJ/kg.

NOMENCLATURE

A = area

C_D = drag coefficient for sphere (~1)

D_0 = diffusion coefficient between H_2 and H_2O

D = diameter

E_m = mixing energy

g = gravitational acceleration

h = heat transfer coefficient

H_C = depth of the water pool

i_{fg} = latent heat of vaporization

m'' = mass flux (kg/m$^2\cdot$s)

N = number of moles

ΔP = steam partial pressure difference between the ambient and at the fuel surface

q'' = heat flux

R_0 = universal gas constant

T = temperature

T_1 = $(T_{sat} + T_f)/2$

v = velocity

V = volume

W_{H_2} = mass flux of H_2 generation

α = void fraction

δ = vapor film thickness

ρ = density

Subscripts

b = breakup

c = coolant

d = displaced

FR = fuel fragment

f = fuel

H_2 = hydrogen

M = mixture

v = vapor

sat = saturated

ACKNOWLEDGMENT

This work was supported by SNL.